We are IntechOpen, the world's leading publisher of Open Access books
Built by scientists, for scientists

6,900
Open access books available

185,000
International authors and editors

200M
Downloads

154
Countries delivered to

Our authors are among the

TOP 1%
most cited scientists

12.2%
Contributors from top 500 universities

CLARIVATE ANALYTICS
BOOK CITATION INDEX
INDEXED

WEB OF SCIENCE™

Selection of our books indexed in the Book Citation Index
in Web of Science™ Core Collection (BKCI)

Interested in publishing with us?
Contact book.department@intechopen.com

Numbers displayed above are based on latest data collected.
For more information visit www.intechopen.com

Perovskite Materials for Resistive Random Access Memories

Jiaqi Zhang and Wubo Li

Abstract

Resistive random access memory (RRAM) utilizes the resistive switching behavior to store information. Compared to charge-based memory devices, the merits of RRAM devices include multi-bit capability, smaller cell size, and energy per bit (~fJ/bit). In this chapter, we review different perovskite material-based resistive random access memories (RRAMs). We first introduce the history of RRAM development and operational mechanism of conduction, followed by a review of two types of materials with perovskite crystal structure. One is conventional perovskite oxides (PCMO, a-LCMO, etc.), and the other is perovskite halides (organic-inorganic hybrid perovskites and inorganic perovskites) that have recently emerged as novel materials in optoelectronic fields. Our goal is to give a comprehensive review of perovskite-based RRAM materials that can be used for neuromorphic computing and to help further ongoing development in the field.

Keywords: memory devices, RRAM, perovskite oxides, perovskite halides, memristors

1. Introduction

Resistive random access memory (RRAM) devices use the resistance switching (RS) behavior to save information, which has attracted much attention due to its outstanding performance compared with traditional semiconductor electronic devices. In comparison to charge-based memory cells, RRAM device possesses various advantages, such as multi-bit capability, simpler device structure (electrode/active layer/electrode), as well as lower energy consumption (~fJ/bit) [1]. Another advantage of RRAM is its good compatibility to the conventional CMOS, which allows it to be integrated into current integrated circuit (IC) technology [2].

RRAM has various potential applications. First, RRAM is considered as the most promising candidate as the next-generation memory device because it acts excellently as both main memory and working memory. As main memory, RRAM is nonvolatile with high memory capacity. As working memory, the operation voltage and power of RRAM are very low, and the write/erase rate is very high. Apart from the memory application, RRAM is also utilized in low-energy-consumption computing as nonvolatile logic circuit [3, 4] and in neuromorphic computing as a synaptic cell, with the latter being a research hotspot in recent years [1].

A typical RRAM device is a metal/insulator/metal (MIM) stack, in which an insulating active layer is sandwiched between the top and the bottom metal electrodes, as shown in **Figure 1**. The device resistance can be tuned by applying an
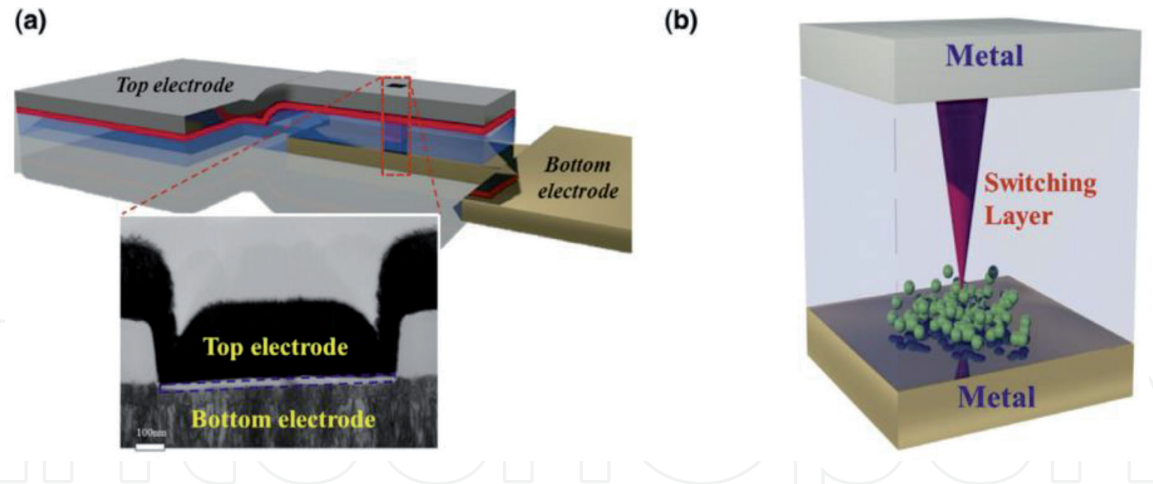
Figure 1.
(a) Schematic diagram of an RRAM device; (b) cross-sectional view of a RRAM device with conductive filament mechanism. Reproduced with permission [2]. Copyright 2016, Elsevier.

electric bias across two electrodes, forming high resistance state (HRS) and low resistance state (LRS). So the nonvolatile memory phenomenon in RRAM device is realized by electrically modulating the RS between HRS and LRS.

The transformation from HRS to LRS is normally named the Set process, and the transformation from LRS to HRS is named the Reset process. There are three kinds of RS switching behaviors. One is unipolar switching, in which the Set and Reset processes can happen at the same polarity of the external bias. Second is bipolar switching, in which RS switching occurs at different polarities of the applied bias. The third is nonpolar resistive memory, in which both RS switching from HRS to LRS and RS switching from LRS to HRS can be achieved without altering the voltage polarity (unipolar), while they can also be achieved by altering the polarity (bipolar).

The schematic I-V characteristics of unipolar switching and bipolar switching are illustrated in **Figure 2**, respectively. In addition to the Set and Reset processes, a Forming process typically exists for many initially prepared RRAM devices, in which an applied forming voltage (V_{form}) drives the formation of CFs with the compliance current limitation. The forming process is normally accomplished before the RRAM device enables to work, and the V_{form} is usually larger than the setting voltage (V_{set}).
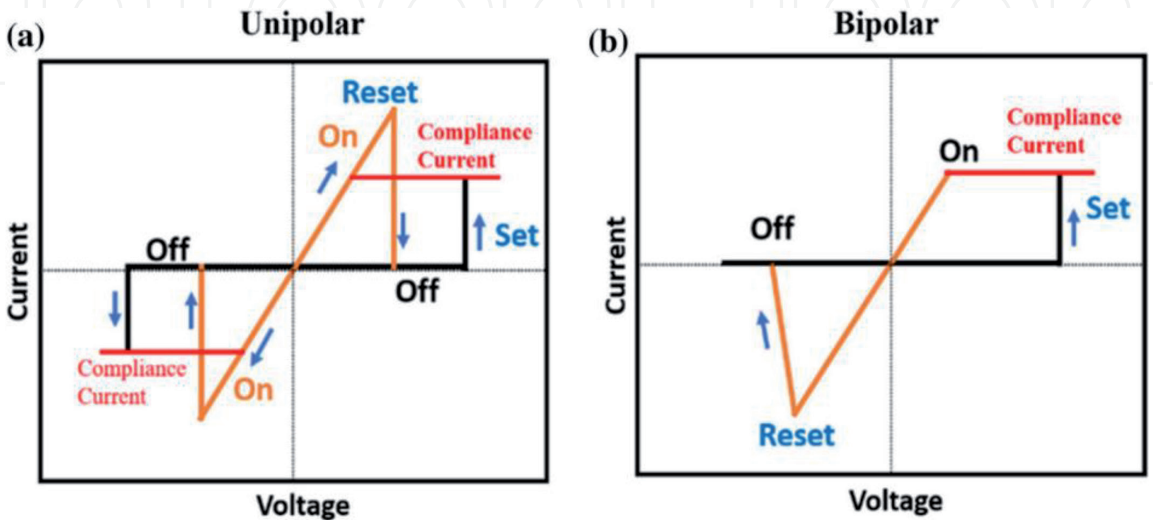

Figure 2.
Typical current voltage (I-V) characteristics of memory devices with (a) unipolar switching and (b) bipolar switching. Reproduced with permission [1]. Copyright 2018, Springer.

As aforementioned, a basic RRAM device usually consists of two electrodes and an active layer. The top and bottom electrodes can use various materials, including elementary substantial metals (Ag, Cu, Al, Au, Pt, W, etc.) [5], metallic alloys (Pt-Al, Cu-Ti, etc.) [6], and oxides (ITO, $SrRuO_3$, Nb:$SrTiO_3$, etc.) [7–9]. Based on the functions in RS conversion, the electrode materials can be divided into two types. One is active electrodes (Cu, Ag, etc.), which contribute to the RS conversion by the migration and/or redox reaction of the electrode ions around the electrode/active layer junction. The other is inert electrodes (Pt, Au, etc.), which do not directly participate in the RS conversion.

As for the active layer, various materials have been utilized in memory devices, such as amorphous metal oxides, polymers, hybrid composites, perovskite oxides, and perovskite halides [10, 11]. The material choice of RRAM active layer has significant influence on the device performance. In this chapter, we will mainly introduce oxides and halides with perovskite structures. Perovskite oxides are a conventional active material family for memories. In addition to high-endurance, chemically stable, and high-speed operation, the strong electron correlation induces many unique properties for perovskite oxides, which makes it remain as one of the most promising materials for RRAM yet. Compared with conventional RRAMs, perovskite halides can make flexible devices with low-cost fabrication, compositional flexibility, and excellent optoelectronic properties, enabling the perovskite halides as a promising next-generation memory material family. Next, we will introduce the memory devices with perovskite oxides and halides separately.

2. Perovskite oxide memory devices

In 2002, perovskite oxide $Pr_{0.7}Ca_{0.3}MnO_3$ was firstly utilized in a 64-bit RRAM array by a 500-nm complementary metal oxide semiconductor (CMOS) process [1]. Nearly two decades passed, transition metal perovskite oxides are still one of the best materials for RRAM active layers. Perovskite oxides possess stable crystal structure with high defect tolerance and structure flexibility, which enables the accommodation of nonstoichiometric ions. The nonstoichiometric ions contribute to the local ionic migration and thermochemical reaction therefore allowing for the RS conversion. In addition, the strongly correlated electrons in perovskite oxides provide various electronic phases and bring out multifunctionality, e.g., colossal magnetoresistance/electroresistance, ferroelectricity, multiferroics, superconductivity, etc. [12]. Also, the competing behavior among different electronic phases brings out the metal-insulator transition (MIT) phenomenon, which allows a significant change of resistance with a tiny electric stimulus [12, 13]. In the following, based on different resistance switching mechanisms, we will introduce RRAM with transition metal perovskite oxides via filament mode and uniform mode, respectively.

2.1 Conductive filament mechanism

Conductive filament (CF) is the most common mechanism to explain the resistance switching of memristor devices, in which the formation and the breakage of filaments are in Set and Reset process, respectively. Many works have proven the conductive filament in RRAM devices. For instance, a co-doped $BaTiO_3$-based device is forming as LRS, and the top electrode is divided into two portions (TE-I and TE-II). Then people measured the resistance between the bottom electrode and TE-I or TE-II. Significantly different resistances are found for two parts, which indicates inhomogeneous conductivity inside the whole memory device [14]. Besides, in an $YMnO_3$-based memory device, people found that the switching I-V curves of

devices with various electrode areas are not remarkably different and that the lateral distribution of filaments is not uniform [15]. Real-time observation of conductive filament was also conducted by TEM in oxide-based memory devices, which shows direct evidence of conductive filament mechanism [16, 17].

Next, we will give a brief introduction on the microscopic mechanisms of filaments, mainly including two types: ion migration and metal-insulator transition.

2.1.1 Ion migration

For the conductive filaments caused by ion migration, the presence of CFs is very random owing to the random distribution of ions and defects in the active layer. Therefore, the formation and rupture of the CFs are strongly dependent on the initial distribution of ions and defects. For bipolar RRAM devices, the microscopic mechanism of ion migration can be classified into three types.

First, the filament is formed by the local redox reaction of metallic cations from the active metal electrode. For example, in an Ag/a-LSMO (amorphous Sr-doped $LaMnO_3$)/Pt device, Ag is demonstrated as the main component of the CFs [18]. When a positive bias is applied to the Ag electrode, some Ag atoms around the Ag/a-LSMO interface will be oxidized into Ag cations, and these Ag cations will move toward the opposite cathode under the external electrical field and are eventually reduced back to Ag atoms around the cathode/a-LSMO interface, therefore forming the CFs between two electrodes. Now if we apply a negative bias to the Ag electrode, the Ag atoms around the cathode will be re-oxidized into Ag^+ and move back toward the Ag electrode, thus leading to the breakage of the filaments. A typical RRAM device of this mode is an insulating active layer sandwiched between an active metallic electrode and an inert electrode [17].

A second mechanism of ion migration is that the positive-charged defects drift under the external voltage. The charged defects, such as oxygen vacancies and excess cations, can tune the Fermi level and correspondingly change the electrical conductivity in the local area. For instance, in a TiO_2-based memory device, the filaments are formed by the oxygen-deficient Ti_4O_7 phase under positive voltage [19]. When applying a negative voltage, the reverse redox occurs with the backward electric field and the parasitic Joule heating and consequently leads to the rupture of CFs [20].

Redox reactions both exist in the aforementioned two microscopic mechanisms. However, bipolar RS phenomenon also can be caused by the ion migration without redox. Pt/NSTO (Nb-doped $SrTiO_3$) device is taken as an example. Under electrical field, the movement of oxygen vacancies can change the Schottky barrier height and the depletion width of the Pt/NSTO junction at some local areas of the interface, resulting in the change of the electrical conductivity alongside the Pt/NSTO interface [21, 22].

For unipolar RS behavior with ion migration, the rupture of the CFs is different from that in the bipolar counterparts. In bipolar devices, the filament rupture is caused by the retraction of the initially moved ions or by the change of interfacial junction barriers. However, in unipolar memory devices, the filament rupture is driven by the Joule heat-assisted thermochemical reaction. For example, in a Au/$YMn_{1-\delta}O_3$/Pt unipolar memory device, after the filament is formed under forward bias, a reverse bias with a similar value cannot supply sufficient energy to retract the initially migrated ions and activate the local reverse redox [15]. Instead, the electrical current can provide enough Joule heat in local areas of the filament; sometimes the local temperature can be increased by several hundreds of Kelvin [15, 23], thus assuring the local reverse redox and the corresponding rupture of CFs. As for the HRS to LRS transformation, accompanied by the ion migration, the electron

hopping barriers and the related trapping states which exist in HRS are removed by the further increase of the applying voltage [15, 17, 24]. The same mechanism has also been proven in the Au/co-doped $BaTiO_3$/Pt unipolar memory device [14].

2.1.2 Metal-insulator transition

Metal-insulator transition (MIT) effect has been found in many perovskite oxides, in which the electronic charges are injected into the insulating material to induct the current with an external bias [25–27]. $Pr_{1-x}Ca_xMnO_3$ (PCMO), now one of the most developed memory materials for neuromorphic computing, is taken as an example, in which resistive switching behavior was first discovered in late 1990s [25]. The electron injection distorts the superlattice structure and the mixed valence band in the strongly electronic correlated PCBM system, which acts as an ion doping process. The rebuilding of the electronic phase separation state can also contribute to the MIT, induced by the external electrical stimulus and parasitical Joule heating, which exhibits CFs-based unipolar RS phenomenon [28]. In addition, filament-type RS behavior may also derive from the Mott transition, which has been demonstrated in many transition metal perovskite oxides [26, 29, 30].

2.2 Uniform resistance switching

In CF-based memory devices, the conductive filaments are formed under electric stimuli in local areas. The I-V characteristics are not proportional to the electrode area due to the random distribution of the filaments. Apart from the CF-based RRAMs, uniform resistance switching mechanism has already been demonstrated, in which the device resistance variation is spatially uniform. Thus the variations of HRS and LRS are both proportional to the electrode area. Uniform RS behavior mainly includes two types, one is the carrier trapping/detrapping, and the other is the ferroelectric polarization.

Carrier trapping/detrapping and the migration of charged defects can tune the Schottky barrier at the metal-insulator interface thus modulating the device resistance. This modulation could occur in local regions near the interface (i.e., filament mode) or occur laterally uniform near the interface (i.e., uniform mode), which is strongly dependent on the interfacial electrical and morphological uniformity. A smooth interface with uniform distribution of charges and defects may bring out uniform RS. Otherwise, filaments may tend to form with nonuniform interfaces. Researchers found that the uniform migration of charged defects (e.g., oxygen vacancies) is too slow thus leading to very slow RS [31]. Nevertheless, the charge trapping/detrapping at the junction can be very fast, enabling uniform RS with fast response, which has been confirmed in the Au/Nb-doped $SrTiO_3$ heterojunction [14].

For the uniform RS by ferroelectric polarization, ferroelectric tunnel junctions (FTJs) are utilized for the RRAM devices, including a ferroelectric tunnel barrier sandwiched by two electrodes. Many perovskite oxide materials have been utilized in the FTJ-based memory devices, such as Pt/$BaTiO_3$/$SrRuO_3$ [8], Pt/$BiFeO_3$/$SrRuO_3$ [32], Co/$BaTiO_3$/$La_{0.7}Sr_{0.3}MnO_3$ [33], etc. The polarization at the ferroelectric/metal junction has a significant influence on the junction barrier profile and modulates the electron tunneling. Thus when the polarization is varied with the external electric field, the resistance state is obviously changed.

Although uniform RS behavior exhibits many advantages, currently the practical application of uniform-type memory devices is still restricted by some intrinsic demerits. The key issue is that the uniform-type device performance is closely dependent on the quality of the films and the junction [6]. For the carrier trapping-/detrapping-based devices, the LRS and the HRS often show considerable relaxation, which deteriorates

the device performance [9]. An effective interfacial modification is commonly required to solve this problem. For the FTJ-based devices, the tunneling current tuned by the polarization is normally remarkably small, which hinders its actual application. In addition, the ferroelectric layer is usually ultrathin, and how to maintain the ultrathin film uniformity in a large scale is another technical issue.

3. Perovskite halide memory devices

In recent years, halide perovskites (HPs) have become a star material due to its excellent optical and charge transport properties. The rapid advance in power-conversion efficiency (PCE) of perovskite solar cells has exceeded by 20% [34], and the simple and solution-based preparation enables low-cost production. HPs have excellent electron migration ability and good optical absorption. With the development of HPs, the hysteresis in the current voltage curve was observed and described [35]. It is found that the hysteresis has a strong dependence on the voltage scanning rate and transient response. Ion migration is thought to be a possible origin of the slow response [36]. This discovery paves the way for HPs' applications in other electronic devices, for example, resistive switching memory (memristors) [37–39], field-effect transistors [40–42], and artificial synapse devices [43, 44]. Owing to its unique features and manufacturing advantages, rapid progress has been made, and HPs are considered as a promising candidate for the next generation of electronic devices [45, 46].

3.1 Tunable bandgap

The perovskite material is an ABX_3 compound with a 3D framework (**Figure 3a**), where A is a monovalent cation. A-site can be an inorganic or organic cation, for example, methylammonium (MA^+, $CH_3NH_3^+$), formamidinium (FA^+, $HC(NH_2)^{2+}$), or Cs^+; B is a divalent cation, and X is an anion. B is typically Pb (also Sn) and X is a halide such as Cl, Br, or I. Based on the composition flexibility of
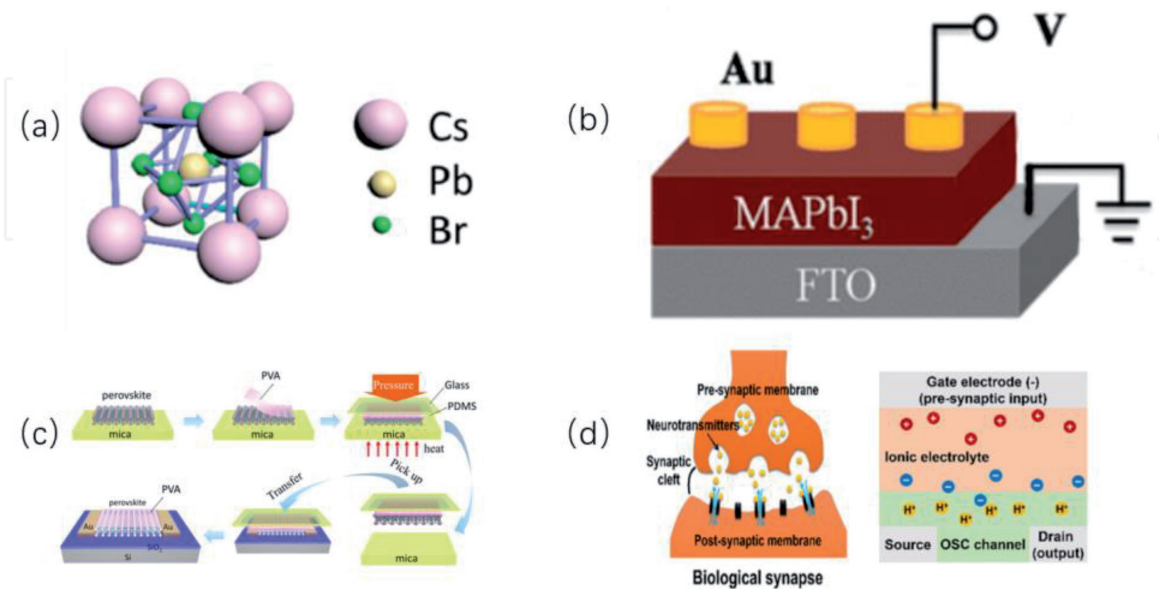

Figure 3.
(a) Crystal structure of HPs [47]. (b) A schematic diagram of device structure halide perovskite memory [48]. (c) FETs based on $CsPbBr_3$ and fabrication method [47]. (d) Biological synapse compared to artificial synapses [49]. (a, c) Reproduced with permission [47]. Copyright 2015, American Chemical Society. (b) Reproduced with permission [48]. Copyright 2018, American Chemical Society. (d) Reproduced with permission [49]. Copyright 2019, American Chemical Society.

HPs, the bandgap can be tuned by replacing elements at each position. In addition, the bandgap can be tuned by controlling the crystalline structure of HPs and the grain size [50].

It is a feasible method to change the length of the bonds between A and B/C sites. In theory, the crystal lattice of the perovskite ABX_3 is expandable, and the gap of the forbidden band is narrow. For example, the material obtained by replacing the MA^+ in the $MAPbI_3$ with an ethylamine, a propylamine, a long-chain alkyl, or an arylamine cation is generally a two-dimensional layered structure. The length of alkylammonium cations at position A was reported in 1990 by Calabrese et al., and the synthesized HPs demonstrated a two-dimensional layered structure [51]. With the increase of the length of cation at site A, the maximum absorption peak is red-shifted from 390 to 450 nm [51]. The modulation of the perovskite bandgap by the substitution of A-site has been demonstrated by the density functional theory (DFT), showing an obvious change, i.e., FA (1.5 eV), MA (1.55 eV), and Cs (1.73 eV) [52, 53]. The angle of B-X-B bond in perovskite structure plays an important role in regulating the bandgap of perovskite materials. Therefore, the change of different metal ions (B) to regulate the structure and properties of perovskite materials is also of great concern. By substituting Pb by Sn at B site, $MASnI_3$ (1.3 eV) exhibits a smaller bandgap than $MAPbI_3$ (1.55 eV) [53]. For the X site, when I ions in $MASnI_3$ are doped with Br in different proportions, the bandgap of the materials can be modulated between 1.3 and 2.15 eV, and the corresponding absorptions are between 950 and 650 nm [54].

Another important way to adjust the bandgap is to control the quantum confinement in the nanoscale. Compared with 0D quantum dots or 1D nanowires, 2D geometry provides a natural way to accurately control the thickness of quantum wells for perovskite halides, resulting in a confinement effect. Huang et al. found that a two-dimensional $MAPbBr_3$ perovskite layer could be regulated by the concentration of oleic acid and the balance between surfactant and precursor in two phases [55]. Two-dimensional $MAPbBr_3$ nano-sheets with different layers show different representative absorption spectra and photoluminescence spectra [55].

3.2 Ion migration

Many perovskite photovoltaic cells have exhibited I-V hysteresis behavior, as shown in **Figure 4** [36, 56, 57]. Ion migration is thought to be an origin of the photocurrent hysteresis. Low formation energy of ionic defects combined with low activation energy for ion migration enables easy and fast ion migration in perovskite halide materials. Although raising potential stability is an issue in HP solar cells, the ion migration combined with the excellent optical and electrical properties of the material also provides an opportunity for new devices such as optically controlled memory and switched diodes.

HPs are good ionic conductors with fast ion migration ability. There are many factors affecting ion migration, such as component ions, defects, cation rotation, etc. We first briefly introduce the defect ions in perovskite crystals. HPs possess various intrinsic point defects, such as vacancies, interstitial defects, and antisite defects. Shao et al. found that ion migration at grain or grain boundary of $MAPbI_3$ perovskite membrane is different [58]. Ion migration in perovskite membranes can be regulated by the introduction of other foreign substances into grain boundaries, such as large fullerene derivatives ($PC_{60}BM$) or small chloride ions [59, 60]. The modulation of ion migration is desirable for the development of high-performance perovskite-based optically adjustable resistors and synaptic devices [60]. Perovskite has been proven as an excellent ion conductor. Because of the ion motion, the semiconductor material can be changed from p-doped to n-doped.
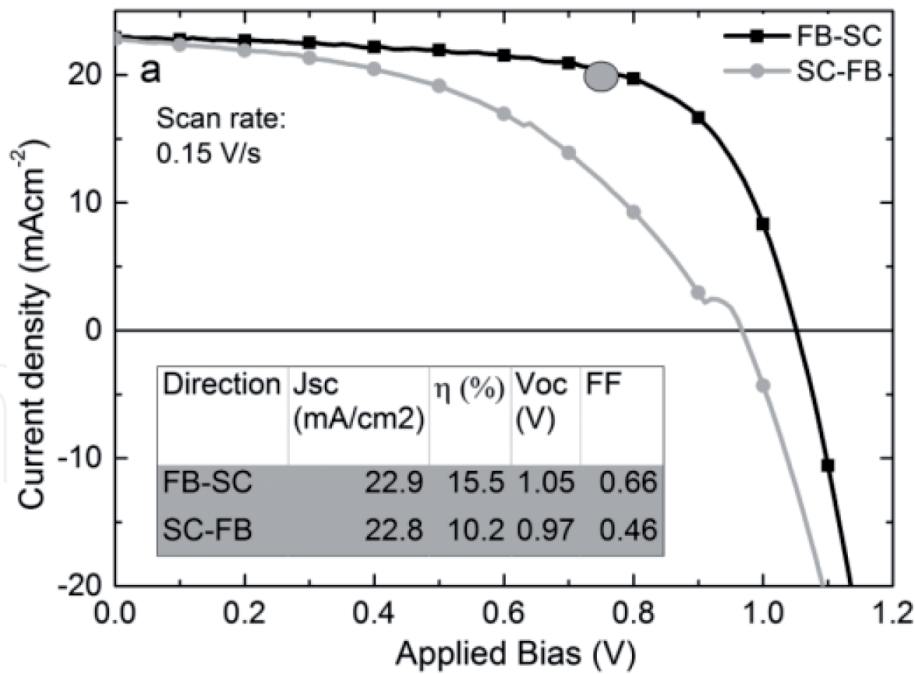
Figure 4.
A typical I-V hysteresis behavior of perovskite solar cells, with forward bias to short circuit sweep (FB-SC) and short circuit to forward bias sweep (SC-FB) [36]. Reproduced with permission [36]. Copyright 2014, American Chemical Society.

By applying external bias, the device structure can be changed from p-i-n structure to n-i-p structure, thus gradually changing the resistance of the device. This memory characteristic of perovskite materials can simulate the signal processing, learning, and memory functions of the nervous system [61]. Perovskite memristors can reduce the energy consumption required for the primary signal transmission of artificial synaptic devices to femto-Joule/(100 nm)^2 which is similar to the ultralow energy consumption required for primary signal transmission in biological synapses. Due to the excellent optical and electrical properties of perovskite materials, some biological functions read by optical signals have also been discovered [62].

3.3 Flexibility

Flexible devices have enormous potentials for applications in emerging areas such as wearable electronics, portable chargers, remote power supplies, automobiles, and aircrafts. The fabrication of the substrate is very important for the flexibility of the final device, and the flexible device based on the polymer substrate is usually needed, resulting in general processing, and manufacturing only in low-temperature environments cannot withstand high-temperature processes. But HP materials do not require high temperatures and can be processed at low temperatures, and HPs provide mechanical flexibility. These make HPs a great advantage in flexible device applications (**Figure 5**). For typical HPs, MAPbBr$_3$, they have weak interactions between organic elements. This combination is relatively weak, so the shear between perovskite surfaces is easy to occur, which explains why this perovskite can provide elasticity under mechanical deformation. The annealing temperature of HPs is generally only one hundred degrees. Therefore, high flexible polymer substrates can be used in HP-based flexible devices because of the low processing temperature. Many repeated bending tests of HP solar cells and storage devices have been reported. These studies show that the materials have a good mechanical flexibility.
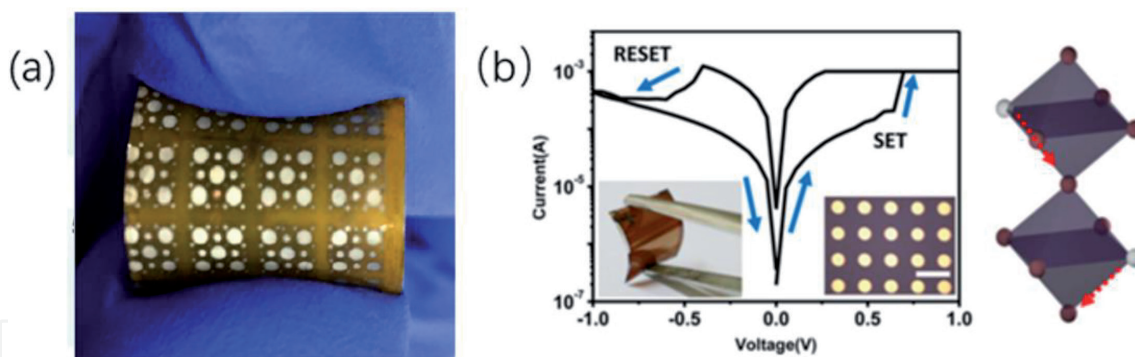
Figure 5.
(a) Photograph of a flexible RRAM device with the Al/CsPbBr$_3$/PEDOT:PSS/ITO structure [63]. (b) Memory device based on flexible substrate of the Au/perovskite/ITO structure and I-V characteristics [37]. (a) Reproduced with permission [63]. Copyright 2017, American Chemical Society. (b) Reproduced with permission [37]. Copyright 2016, American Chemical Society.

HP-based flexible resistive switch storage device has been fabricated on a plastic substrate. After more than 100 times of bending radius of 1.5 cm, the storage device still has electrical performance (**Figure 5b**) [37]. The first fiber-shaped perovskite memristor was developed in 2016 [64]. In particular, fiber morphology is expected to promote the application of perovskite materials in wearable memory and computing device. Therefore, thanks to the good mechanical and electrical reliability, HP-based devices are very promising for the next-generation flexible memory devices.

3.4 Thin film preparation methods

In the field of perovskite solar cells, it is necessary to improve the photoelectric conversion efficiency of perovskite solar cells with good thin film preparation technology [65, 66]. Generally good perovskite thin films have smooth surface and large grain size with relatively few defects. In order to achieve high-performance devices, controlling the uniformity, thickness, and grain size of the HP layer is of great importance in the fabrication process.

In the early preparation of the solar cell, the perovskite precursor solution is usually spin-coated on the hydrophilic TiO$_2$ layer, and due to the hydrophilicity, the perovskite is easily deposited on the TiO$_2$ [67, 68]. Resistive switch memory and logic device is a kind of device with an insulating layer sandwiched between two metal layers. Thus when we use a solution method to prepare HP layers for the memristor devices, the perovskite precursor solution needs to be deposited on the hydrophobic metal layer. However, it is difficult to use the solution method to deposit a HP film on a hydrophobic metal surface. Because of the hydrophobicity of metal electrodes, for example, a simple spin coating method of MAPbI$_3$ precursor solution may produce island growth on the metal surface. One-step spin coating therefore is not suitable for the fabrication of memory and logic device structures without interfacial modification. In order to solve this problem, the surface of metal electrode is usually treated with ultraviolet ozone (UVO) or O$_2$ plasma to change the hydrophobicity of metal electrode. However, it is still not easy for HP thin films to get a good uniformity, both in one-step spin coating and two-step spin coating. This mainly originates from the difference between the general perovskite layer annealing temperature and the solvent boiling point temperature. For example, the annealing temperature of MAPBI$_3$ is generally 100–150°C, while for the solvent perovskite, such as γ-butyrolactone and N,N dimethylformamide, possessing high boiling points of 204 and 153°C, respectively [44]. Thus the nucleation during the

substrate annealing could be very slow, which tends to achieve poor film morphology, such as cracks or even pores. Anti-solvent engineering can be applied in spin coating process to eliminate this issue. In anti-solvent engineering, toluene, chloroform, and other substances are often used as anti-solvents. Because they are insoluble to perovskite, when anti-solvent is added, the anti-solvent begins to diffuse and permeate into HPs solution. It is helpful for rapid nucleation. Anti-solvent engineering has been successfully used in the fabrication of HP-based flexible resistive switch memory [37]. However, the use of anti-solvent engineering will also bring some problems. With the addition of anti-solvent, it gradually begins to diffuse and permeate in HP solution. However, it is not possible for the anti-solvent to diffuse and penetrate uniformly throughout the perovskite film, which may result in a large distribution of the perovskite crystal size throughout the film. In order to prepare more uniform membranes, it is usually necessary to add additives such as alkane dimercaptan to control the crystallization kinetics of perovskite [69].

3.5 HPs for resistive switching memories

With the advent of the information age and the rapid development of the Internet, the information that needs to be stored has been explosively increased, and the traditional storage equipment is more and more difficult to meet the demand. As a new-generation storage device, the memristor has great potential in the field of storage. In terms of storage performance, excellent memory devices need to have the advantages of fast working time, long service life, low power consumption, and low cost.

For memristor applications, many materials have been used, from organic materials and binary metal oxides to perovskite halide. Among them, metal oxide-based resistive switch devices have been extensively studied and applied in many fields. However, the technology has many demerits, such as high-power consumption and complicated fabrication process, which is not suitable for fabrication of flexible/wearable devices. As discussed above, perovskite halides are an ideal alternative to fabricate flexible devices [46].

For example, the change in the resistance switching for the $MAPbI_3$ memristor is a filament-type mechanism with the direct reaction of the charge carriers with the defects [39]. For RRAMs, fast charge transfer can reduce energy consumption. In HPs, the carrier transport capacity can be enhanced with appropriate concentrations of defects. For instance, doping $MAPbI_3$ with Br reduces the "SET" voltage, thereby reducing the power consumption of the device. This is because the activation energy of ion migration with Br vacancies is smaller than that with I. Thus, the HRS to LRS switching energy is reduced, and the switching response is accelerated.

At mentioned above, anti-solvent engineering has been utilized in the preparation of HP thin Films. The $MAPbI_3$ thin films treated with toluene as anti-solvent exhibit extremely low electric field about 3.25×10^3 V/cm and high switch-specific resistance switching behavior [70].

As a low-cost material, HPs have a great potential for the development of wearable and portable devices. Yan et al. developed the first fiber-shaped perovskite memristor [64]. In particular, fiber morphology is expected to promote the application of perovskite materials in wearable memory and computing device.

As the volume of information increases, devices that can store more data in the same size are the trend in the future. So, it is important to develop the memory device into a device with high storage density. Hwang et al. fabricated $MAPbI_3$ layer for nano-RRAM devices on 250 nm perforated silicon wafers by vapor deposition [71]. The device has the characteristics of bipolar resistance switch, low operating voltage, high switching speed (200 ns), high durability, and high data retention

time (>10^5 s). In addition, the continuous vapor deposition technology is extended to $MAPbI_3$ memristor with a cross-point array structure. This method enables large area device fabrication for high-density memory devices [71].

All-inorganic perovskite halides, such as $CsPbBr_3$, have also demonstrated as working flexible nonvolatile memories, with a filament-type RS mechanism (**Figure 6a**) [63]. $CsPbBr_3$ quantum dots are also developed for the memory cells [73, 74]. Besides, due to lead in HPs being a component that pollutes the environment and is harmful to humans, it is also necessary to develop lead-free devices. Han et al. successfully fabricated RRAMs based on lead-free inorganic cesium iodide ($CsSnI_3$) perovskite material, as shown in **Figure 6b** [72]. Some typical HP-based RRAMs are compared, as shown in **Table 1**.

In addition to the traditional perovskite halides with ABX_3 structure, other new types of materials have also been utilized in memory devices. 2D perovskite is another promising candidate for RRAM. The conductivity of HPs is low, but it has a good carrier transport ability. At present, most of the HP RRAMs are based on 3D $MAPbX_3$ and some 2D Ruddlesden-Popper (RP) phase perovskite. 2D perovskite material has high Schottky barrier, 2D anisotropic structure, and electrothermal activation energy characteristics. Compared with 3D perovskite devices, the off current of 2D perovskite devices can be greatly reduced. Tian et al. reported the utilization of single-crystalline 2D $(PEA)_2PbBr_4$ and graphene for RRAM [76]. The two sides of 2D HPs are entrapped by graphene and Au, respectively. Due to the low conductivity of 2D HPs caused by multilayer organic ligands, there is no leakage current channel in perovskite grain boundaries of 2D HPs. The off current is limited to 1 pA. It is proven that the switching behavior has good reproducibility by switching devices at 10 pA program current circulate 100 times. Cheng et al. fabricated into Al/2D $(CH_3NH_3)_2PbI_2(SCN)_2$ perovskite film/indium-tin oxide [78]. The RRAM shows ternary switching. The three states have a conductivity ratio of $1:10^3:10^7$, with long retention over 10,000 s. A transparent 2D perovskite $(C_4H_9NH_3)_2PbBr_4$ has also been developed for compliance-free multilevel RS devices [79]. Ultrathin bismuth halide $Cs_3Bi_2I_9$ is also used as an electronic memory device with a typical bipolar RS behavior [80].

For most exploited devices, the data only transiently converts the optical signal into a circuit under illumination, which requires the use of additional converters to further store the output signal and record the occurrence of optical stimuli. HPs have a very strong optical absorption ability, low exciton binding energy, and long life carrier transmission time, so HPs can display a short signal under illumination, which can be used in light-stimulated devices. Chen et al. first introduced the concept of floating gate flash memory and successfully fabricated HP floating gate photomemory with a multilevel memory behavior [81]. Wang et al. first introduced a photonic RRAM based on $CsPbBr_3$ quantum dots. The $CsPbBr_3$ quantum dot layer
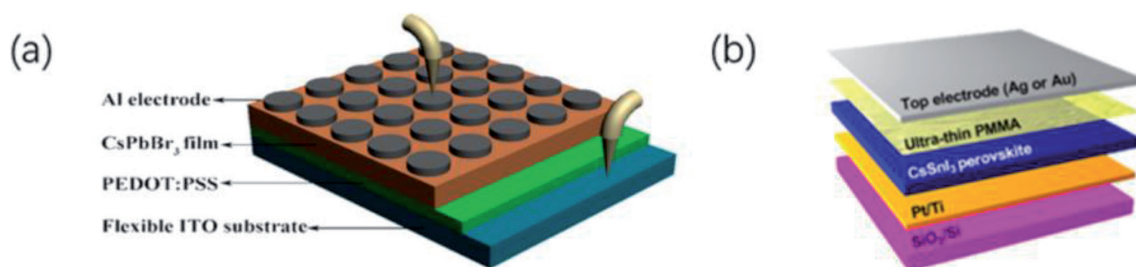

Figure 6.
(a) Schematic drawing of the $CsPbBr_3$-based flexible resistive switching memory [63]. (b) Schematic diagram of the Ag or Au/PMMA/$CsSnI_3$/Pt/SiO_2/Si vertical stack structure [72]. (a) Reproduced with permission [63]. Copyright 2017, American Chemical Society. (b) Reproduced with permission [72]. Copyright 2019, American Chemical Society.

Device structure	Set voltage [V]	On/off ratio	Retention [s]	Endurance [cycles]	Ref.
Au/MAPbI$_{3-x}$Cl$_x$/FTO	0.8	10	1×10^4	10^2	[38]
Ag/MAPbI$_3$/Pt	0.13	10^6	1×10^4	400	[70]
Ni/ZnO/CsPbBr$_3$/FTO	−0.95	10^5	1×10^4	—	[75]
Al/CsPbBr$_3$/PEDOT:PSS/ITO/PET	−0.6	10^2	—	50	[63]
Ag/PMMA/CsPbI$_3$/Pt	0.18	10^6	—	300	[62]
Graphene/PEA$_2$PbBr$_4$/Au	2.8	10	1×10^3	100	[76]
Ag/PMMA/CsSnI$_3$/Pt/SiO$_2$/Si	0.13	10^3	7×10^3	600	[72]
Au/MAPbI$_3$/Au	0.96	10^8	1×10^4	1000	[77]

Table 1.
Summary of hybrid perovskite RRAMs in this review.

is sandwiched by two PMMA layers. Silver is selected as the top electrode by thermal evaporation [82]. In the absence of light, the device displays a bipolar resistive switch memory. By inputting the light field and electric field signals, the current will be used as the output signal to realize the switching logic operation.

The traditional von Neumann architecture requires a large amount of data transmission directly in CPU and memory (memory wall). This leads to increased power consumption. In order to solve this problem, Tian et al. proposed a fully distributed architecture based on optical synapse. The optical synapse based on layered 2D (PEA)$_2$PbI$_4$ perovskite structure was prepared [83]. This 2D perovskite-type optical synapse is similar to the biologic optical synapse with light-induced excitation/inhibition. Based on the unique optical gate control effect, the ultrahigh light response rate can reach 730 a/w. Lead-free 2D perovskite was also utilized for the first time in the study of flexible optical synaptic devices [84]. A flexible optical synapse based on 2D perovskite (PEA)$_2$SnI$_4$ can mimic the short-term plasticity of biological synapses.

In addition to the single device operation, we should also pay attention to cross-array arrangement of RRAMs. A large number of RRAMs can be connected to each other in micro-space to form a cross-array structure. This architecture combines the memory advantage of the RRAMs and the massively parallel processing of the cross array. Cross arrays exhibit the characteristics of large-scale parallel processing, distributed information storage, self-organization, self-adaptation, etc. RRAM cross array provides a more convenient storage structure for binary images and a new storage scheme for gray-scale images. Hwang et al. prepared homogeneous perovskite thin films by sequential evaporation deposition and then prepared 16 × 16 cross-point array of RRAM [71]. The I-V characteristics of the memory cells show a variation among different points, while the setting voltages remain similar, and the on/off ratios are large for all devices. The memory characteristics prove the feasibility of HPs in the application of high-density cross-point memory. Kang et al. fabricated perovskite RRAM devices with high yield in 8 × 8 cross-bar arrays using solution-treated perovskite films [77]. Among the 64 memory cells, 55 cells are functional. These results are of great significance for the practical perovskite storage equipment with low cost and high density through a simple solution.

4. Conclusions

In this chapter, we have outlined an overview of the application of perovskite oxides and perovskite halides in memory devices. In the new era, artificial

intelligence and IoTs are dramatically developing. Correspondingly, memory cells are getting more and more important, especially in low-power information storage and in neuromorphic computing. Although already developing for around two decades, perovskite oxides are still one of the most promising materials for RRAM owing to its high-endurance, chemically stable, and high-speed operation. However, more efforts are expected for perovskite oxide-based memories. Technologically, improving the endurance of the RS is still required for better actual application. Fundamentally, the basic operational mechanism of perovskite oxide RRAM device needs further investigation, especially considering the strong electron correlation system. For the perovskite halide, as a rising star, it has exhibited a great potential in the application of memristors. Flexible devices, low-cost fabrication, compositional flexibility, and excellent optoelectronic properties enable the perovskite halides to obtain potential application into wearable memory devices and artificial synapse. However, the film quality of HPs should be further improved, because the memory device performance is significantly dependent on the film uniformity. In addition, the intrinsic stability issue needs to be addressed by intended doping and interfacial passivation. Overall, further investigation is required to fulfill the expectation on these promising materials for the next-generation electronics.

Acknowledgements

Conflict of interest

The authors declare that they have no conflict of interest.

Author details

Jiaqi Zhang* and Wubo Li
Key Laboratory of Automobile Materials of MOE, College of Materials Science and Engineering, Jilin University, Changchun, China

*Address all correspondence to: zhangjiaqi@jlu.edu.cn

IntechOpen

References

[1] Hong XL, Loy DJJ, Dananjaya PA, Tan F, Ng CM, Lew WS. Oxide-based RRAM materials for neuromorphic computing. Journal of Materials Science. 2018;**53**:8720-8746. DOI: 10.1007/s10853-018-2134-6

[2] Chang TC, Chang KC, Tsai TM, Chu TJ, Sze SM. Resistance random access memory. Materials Today. 2016;**19**:254-264. DOI: 10.1016/j.mattod.2015.11.009

[3] Yang JJ, Strukov DB, Stewart DR. Memristive devices for computing. Nature Nanotechnology. 2012;**8**:13-24. DOI: 10.1038/nnano.2012.240

[4] Zhu D, Li Y, Shen W, Zhou Z, Liu L, Zhang X. Resistive random access memory & its applications in storage & nonvolatile logic. Journal of Semiconductors. 2017;**38**:1-13. DOI: 10.1088/1674-4926/38/7/071002

[5] Gao S, Zeng F, Song C, Pan F, Chen C. Recent progress in resistive random access memories: Materials, switching mechanisms, and performance. Materials Science & Engineering R: Reports. 2014;**83**:1-59. DOI: 10.1016/j.mser.2014.06.002

[6] Yan ZB, Liu JM. Resistance switching memory in perovskite oxides. Annals of Physics. 2015;**358**:206-224. DOI: 10.1016/j.aop.2015.03.028

[7] Zhang J, Wu X, Ma X, Yuan L, Huang K, Feng S. Amporphous La0.75Sr0.25MnO$_3$ thin film fabricated by pulsed laser deposition as a medium layer for semitransparent resistive random access memory. Chinese Journal of Inorganic Chemistry. 2018;**34**:784-790

[8] Wen Z, You L, Wang J, Li A, Wu D. Temperature-dependent tunneling electroresistance in Pt/BaTiO$_3$/SrRuO$_3$ ferroelectric tunnel junctions. Applied Physics Letters. 2013;**103**:132913. DOI: 10.1063/1.4823580

[9] Yan ZB, Liu JM. Coexistence of high performance resistance and capacitance memory based on multilayered metal-oxide structures. Scientific Reports. 2013;**3**:2482. DOI: 10.1038/srep02482

[10] Gao S, Yi X, Shang J, Liu G, Li R-W. Organic and hybrid resistive switching materials and devices. Chemical Society Reviews. 2019;**48**:1531-1565. DOI: 10.1039/C8CS00614H

[11] Liu D, Cheng H, Zhu X, Wang G, Wang N. Analog memristors based on thickening/thinning of Ag nanofilaments in amorphous manganite thin films. ACS Applied Materials & Interfaces. 2013;**5**:11258-11264. DOI: 10.1021/am403497y

[12] Jeong DS, Thomas R, Katiyar RS, Scott JF, Kohlstedt H, Petraru A, et al. Emerging memories: Resistive switching mechanisms and current status. Reports on Progress in Physics. 2012;**75**:076502. DOI: 10.1088/0034-4885/75/7/076502

[13] Waser R, Dittmann R, Staikov G, Szot K. Redox-based resistive switching memories-nanoionic mechanisms, prospects, and challenges. Advanced Materials. 2009;**21**:2632-2663. DOI: 10.1002/adma.200900375

[14] Yan Z, Guo Y, Zhang G, Liu JM. High-performance programmable memory devices based on Co-doped BaTiO$_3$. Advanced Materials. 2011;**23**:1351-1355. DOI: 10.1002/adma.201004306

[15] Yan ZB, Li SZ, Wang KF, Liu JM. Unipolar resistive switching effect in YMn1-δO$_3$ thin films. Applied Physics Letters. 2010;**96**:1-4. DOI: 10.1063/1.3280380

[16] Sun H, Liu Q, Li C, Long S, Lv H, Bi C, et al. Memory switching: Direct observation of conversion between threshold switching and memory

switching induced by conductive filament morphology. Advanced Functional Materials. 2014;**24**:5772. DOI: 10.1002/adfm.201470243

[17] Yang Y, Gao P, Gaba S, Chang T, Pan X, Lu W. Observation of conducting filament growth in nanoscale resistive memories. Nature Communications. 2012;**3**:732-738. DOI: 10.1038/ncomms1737

[18] Liu D, Wang N, Wang G, Shao Z, Zhu X, Zhang C, et al. Nonvolatile bipolar resistive switching in amorphous Sr-doped $LaMnO_3$ thin films deposited by radio frequency magnetron sputtering. Applied Physics Letters. 2013;**102**:134105. DOI: 10.1063/1.4800229

[19] Kwon D-H, Kim KM, Jang JH, Jeon JM, Lee MH, Kim GH, et al. Atomic structure of conducting nanofilaments in TiO_2 resistive switching memory. Nature Nanotechnology. 2010;**5**:148-153. DOI: 10.1038/nnano.2009.456

[20] Larentis S, Nardi F, Balatti S, Gilmer DC, Ielmini D. Resistive switching by voltage-driven ion migration in bipolar RRAM—Part II: Modeling. IEEE Transactions on Electron Devices. 2012;**59**:2468-2475. DOI: 10.1109/TED.2012.2202320

[21] Shang DS, Sun JR, Shi L, Wang ZH, Shen BG. Resistance dependence of photovoltaic effect in $Au/SrTiO_3$:Nb(0.5 wt%) Schottky junctions. Applied Physics Letters. 2008;**93**:172119. DOI: 10.1063/1.3009285

[22] Lee E, Gwon M, Kim D-W, Kim H. Resistance state-dependent barrier inhomogeneity and transport mechanisms in resistive-switching $Pt/SrTiO_3$ junctions. Applied Physics Letters. 2011;**98**:132905. DOI: 10.1063/1.3567755

[23] Strachan JP, Strukov DB, Borghetti J, Joshua Yang J, Medeiros-Ribeiro G, Stanley Williams R. The switching location of a bipolar memristor: Chemical, thermal and structural mapping. Nanotechnology. 2011;**22**:254015. DOI: 10.1088/0957-4484/22/25/254015

[24] Choi JS, Kim J-S, Hwang IR, Hong SH, Jeon SH, Kang S-O, et al. Different resistance switching behaviors of NiO thin films deposited on Pt and $SrRuO_3$ electrodes. Applied Physics Letters. 2009;**95**:022109. DOI: 10.1063/1.3173813

[25] Asamitsu A, Tomioka Y, Kuwahara H, Tokura Y. Current switching of resistive states in magnetoresistive manganites. Nature. 1997;**388**:50-52. DOI: 10.1038/40363

[26] Kim DS, Kim YH, Lee CE, Kim YT. Colossal electroresistance mechanism in a Au/Pr0.7Ca0.3MnO$_3$/Pt sandwich structure: Evidence for a Mott transition. Physical Review B. 2006;**74**:174430. DOI: 10.1103/PhysRevB.74.174430

[27] Meijer GI, Staub U, Janousch M, Johnson SL, Delley B, Neisius T. Valence states of Cr and the insulator-to-metal transition in Cr-doped $SrTiO_3$. Physical Review B. 2005;**72**:155102. DOI: 10.1103/PhysRevB.72.155102

[28] Yan ZB, Wang KF, Li SZ, Luo SJ, Liu J-M. Reversible resistance switching in La0.225Pr0.4Ca0.375MnO$_3$: The joule-heat-assisted phase transition. Applied Physics Letters. 2009;**95**:143502. DOI: 10.1063/1.3241997

[29] Fors R, Khartsev SI, Grishin AM. Giant resistance switching in metal-insulator-manganite junctions: Evidence for Mott transition. Physical Review B. 2005;**71**:045305. DOI: 10.1103/PhysRevB.71.045305

[30] Waser R, Aono M. Nanoionics-based resistive switching memories. Nature Materials. 2007;**6**:833-840. DOI: 10.1038/nmat2023

[31] Jiang W, Noman M, Lu YM, Bain JA, Salvador PA, Skowronski M. Mobility of oxygen vacancy in $SrTiO_3$ and its implications for oxygen-migration-based resistance switching. Journal of Applied Physics. 2011;**110**:034509. DOI: 10.1063/1.3622623

[32] Hong S, Choi T, Jeon JH, Kim Y, Lee H, Joo H-Y, et al. Large resistive switching in ferroelectric $BiFeO_3$ nano-island based switchable diodes. Advanced Materials. 2013;**25**:2339-2343. DOI: 10.1002/adma.201204839

[33] Valencia S, Crassous A, Bocher L, Garcia V, Moya X, Cherifi RO, et al. Interface-induced room-temperature multiferroicity in $BaTiO_3$. Nature Materials. 2011;**10**:753-758. DOI: 10.1038/nmat3098

[34] Green MA, Hishikawa Y, Dunlop ED, Levi DH, Hohl-Ebinger J, Ho-Baillie AWY. Solar cell efficiency tables (version 52). Progress in Photovoltaics: Research and Applications. 2018;**26**:427-436

[35] Unger EL, Hoke ET, Bailie CD, Nguyen WH, Bowring AR, Heumüller T, et al. Hysteresis and transient behavior in current-voltage measurements of hybrid-perovskite absorber solar cells. Energy & Environmental Science. 2014;**7**:3690-3698. DOI: 10.1039/C4EE02465F

[36] Snaith HJ, Abate A, Ball JM, Eperon GE, Leijtens T, Noel NK, et al. Anomalous hysteresis in perovskite solar cells. Journal of Physical Chemistry Letters. 2014;**5**:1511-1515. DOI: 10.1021/jz500113x

[37] Gu C, Lee JS. Flexible hybrid organic-inorganic perovskite memory. ACS Nano. 2016;**10**:5413-5418. DOI: 10.1021/acsnano.6b01643

[38] Yoo EJ, Lyu M, Yun J, Kang CJ, Choi YJ, Wang L. Resistive switching behavior in organic-inorganic hybrid $CH_3NH_3PbI_{3-x}Cl_x$ perovskite for resistive random access memory devices. Advanced Materials. 2015;**27**:6170-6175

[39] Hwang B, Gu C, Lee D, Lee J-S. Effect of halide-mixing on the switching behaviors of organic-inorganic hybrid perovskite memory. Scientific Reports. 2017;**7**:43794

[40] Senanayak SP, Yang B, Thomas TH, Giesbrecht N, Huang W, Gann E, et al. Understanding charge transport in lead iodide perovskite thin-film field-effect transistors. Science Advances. 2017;**3**:e1601935

[41] Wei W, Zhang Y, Xu Q, Wei H, Fang Y, Wang Q, et al. Monolithic integration of hybrid perovskite single crystals with heterogenous substrate for highly sensitive X-ray imaging. Nature Photonics. 2017;**11**:315

[42] Ward JW, Smith HL, Zeidell A, Diemer PJ, Baker SR, Lee H, et al. Solution-processed organic and halide perovskite transistors on hydrophobic surfaces. ACS Applied Materials & Interfaces. 2017;**9**:18120-18126

[43] Xu W, Cho H, Kim YH, Kim YT, Wolf C, Park CG, et al. Organometal halide perovskite artificial synapses. Advanced Materials. 2016;**28**:5916-5922. DOI: 10.1002/adma.201506363

[44] Choi J, Han JS, Hong K, Kim SY, Jang HW. Organic-inorganic hybrid halide perovskites for memories, transistors, and artificial synapses. Advanced Materials. 2018;**30**:1704002. DOI: 10.1002/adma.201704002

[45] Dang VQ, Han G-S, Trung TQ, Jin Y-U, Hwang B-U, Jung H-S, et al. Methylammonium lead iodide perovskite-graphene hybrid channels in flexible broadband phototransistors. Carbon. 2016;**105**:353-361

[46] Kim H, Han JS, Choi J, Kim SY, Jang HW. Halide perovskites for applications beyond photovoltaics. Small Methods. 2018;**2**:1700310

[47] Huo C, Liu X, Song X, Wang Z, Zeng H. Field-effect transistors based on van-der-Waals-grown and dry-transferred all-inorganic perovskite ultrathin platelets. Journal of Physical Chemistry Letters. 2017;**8**:4785-4792. DOI: 10.1021/acs.jpclett.7b02028

[48] Ma H, Wang W, Xu H, Wang Z, Tao Y, Chen P, et al. Interface state-induced negative differential resistance observed in hybrid perovskite resistive switching memory. ACS Applied Materials & Interfaces. 2018;**10**:21755-21763. DOI: 10.1021/acsami.8b07850

[49] Lee Y, Lee T-W. Organic synapses for neuromorphic electronics: From brain-inspired computing to sensorimotor nervetronics. Accounts of Chemical Research. 2019;**52**:964-974. DOI: 10.1021/acs.accounts.8b00553

[50] D'Innocenzo V, Kandada ARS, De Bastiani M, Gandini M, Petrozza A. Tuning the light emission properties by band gap engineering in hybrid lead halide perovskite. Journal of the American Chemical Society. 2014;**136**:17730-17733. DOI: 10.1021/ja511198f

[51] Calabrese J, Jones NL, Harlow RL, Herron N, Thorn DL, Wang Y. Preparation and characterization of layered lead halide compounds. Journal of the American Chemical Society. 1991;**113**:2328-2330

[52] Amat A, Mosconi E, Ronca E, Quarti C, Umari P, Nazeeruddin MK, et al. Cation-induced band-gap tuning in organohalide perovskites: Interplay of spin-orbit coupling and octahedra tilting. Nano Letters. 2014;**14**:3608-3616

[53] Koh TM, Krishnamoorthy T, Yantara N, Shi C, Leong WL, Boix PP, et al. Formamidinium tin-based perovskite with low Eg for photovoltaic applications. Journal of Materials Chemistry A. 2015;**3**:14996-15000

[54] Hao F, Stoumpos CC, Cao DH, Chang RPH, Kanatzidis MG. Lead-free solid-state organic-inorganic halide perovskite solar cells. Nature Photonics. 2014;**8**:489-494. DOI: 10.1038/nphoton.2014.82

[55] Huang C, Gao Y, Wang S, Zhang C, Yi N, Xiao S, et al. Giant blueshifts of excitonic resonances in two-dimensional lead halide perovskite. Nano Energy. 2017;**41**:320-326

[56] Zhang J, Morbidoni M, Huang K, Feng S, McLachlan MA. Environmentally friendly, aqueous processed ZnO as an efficient electron transport layer for low temperature processed metal-halide perovskite photovoltaics. Inorganic Chemistry Frontiers. 2018;**5**:84-89. DOI: 10.1039/C7QI00667E

[57] Zhang J, Tan CH, Du T, Morbidoni M, Lin C, Xu S, et al. ZnO-PCBM bilayers as electron transport layers in low-temperature processed perovskite solar cells. Scientific Bulletin. 2018;**63**:343-348. DOI: 10.1016/j.scib.2018.02.004

[58] Shao Y, Fang Y, Li T, Wang Q, Dong Q, Deng Y, et al. Grain boundary dominated ion migration in polycrystalline organic-inorganic halide perovskite films. Energy & Environmental Science. 2016;**501**:395-398. DOI: 10.1039/C6EE00413J

[59] Shao Y, Xiao Z, Bi C, Yuan Y, Huang J. Origin and elimination of photocurrent hysteresis by fullerene passivation in $CH_3NH_3PbI_3$ planar heterojunction solar cells. Nature Communications. 2014;**5**:1-7. DOI: 10.1038/ncomms6784

[60] Yang B, Brown CC, Huang J, Collins L, Sang X, Unocic RR, et al. Enhancing ion migration in grain boundaries of hybrid organic-inorganic perovskites by chlorine. Advanced Functional Materials. 2017;**27**:1700749

[61] Xiao Z, Huang J. Energy-efficient hybrid perovskite memristors and synaptic devices. Advanced Electronic Materials. 2016;**2**:1-8. DOI: 10.1002/aelm.201600100

[62] Wang Y, Lv Z, Chen J, Wang Z, Zhou Y, Zhou L, et al. Photonic synapses based on inorganic perovskite quantum dots for neuromorphic computing. Advanced Materials. 2018;**30**:1-9. DOI: 10.1002/adma.201802883

[63] Liu D, Lin Q, Zang Z, Wang M, Wangyang P, Tang X, et al. Flexible all-inorganic perovskite $CsPbBr_3$ nonvolatile memory device. ACS Applied Materials & Interfaces. 2017;**9**:6171-6176. DOI: 10.1021/acsami.6b15149

[64] Yan K, Chen B, Hu H, Chen S, Dong B, Gao X, et al. First fiber-shaped non-volatile memory device based on hybrid organic-inorganic perovskite. Advanced Electronic Materials. 2016;**2**:1-7. DOI: 10.1002/aelm.201600160

[65] Yu JC, Kim DB, Baek G, Lee BR, Jung ED, Lee S, et al. High-performance planar perovskite optoelectronic devices: A morphological and interfacial control by polar solvent treatment. Advanced Materials. 2015;**27**:3492-3500. DOI: 10.1002/adma.201500465

[66] Jeon NJ, Noh JH, Kim YC, Yang WS, Ryu S, Il Seok S. Solvent engineering for high-performance inorganic-organic hybrid perovskite solar cells. Nature Materials. 2014;**13**:1-7. DOI: 10.1038/nmat4014

[67] Lee MM, Teuscher J, Miyasaka T, Murakami TN, Snaith HJ. Efficient hybrid solar cells based on meso-superstructured organometal halide perovskites. Science. 2012;**338**:643-647. DOI: 10.1126/science.1228604

[68] Liu M, Johnston MB, Snaith HJ. Efficient planar heterojunction perovskite solar cells by vapour deposition. Nature. 2013;**501**:395-398. DOI: 10.1038/nature12509

[69] Liang P-W, Liao C-Y, Chueh C-C, Zuo F, Williams ST, Xin X-K, et al. Additive enhanced crystallization of solution-processed perovskite for highly efficient planar-heterojunction solar cells. Advanced Materials. 2014;**26**:3748-3754. DOI: 10.1002/adma.201400231

[70] Choi J, Park S, Lee J, Hong K, Kim D-H, Moon CW, et al. Organolead halide perovskites for low operating voltage multilevel resistive switching. Advanced Materials. 2016;**28**:6562-6567. DOI: 10.1002/adma.201600859

[71] Hwang B, Lee J. A strategy to design high-density nanoscale devices utilizing vapor deposition of metal halide perovskite materials. Advanced Materials. 2017;**29**:1701048

[72] Han JS, Van Le Q, Choi J, Kim H, Kim SG, Hong K, et al. Lead-free all-inorganic cesium tin iodide perovskite for filamentary and Interface-type resistive switching toward environment-friendly and temperature-tolerant nonvolatile memories. ACS Applied Materials & Interfaces. 2019;**11**:8155-8163. DOI: 10.1021/acsami.8b15769

[73] Zhou L, Chen X, Han S-T, Zhou Y, Lv Z, Wang Y, et al. Photonic synapses based on inorganic perovskite quantum dots for neuromorphic computing. Advanced Materials. 2018;**30**:1802883. DOI: 10.1002/adma.201802883

[74] Zhang H, Li Q, Song X, Zhang H, Zhang Y, Yu Y, et al. Low-voltage all-inorganic perovskite quantum

dot transistor memory. Applied Physics Letters. 2018;**112**:212101. DOI: 10.1063/1.5028474

[75] Wu Y, Wei Y, Huang Y, Cao F, Yu D, Li X, et al. Capping CsPbBr$_3$ with ZnO to improve performance and stability of perovskite memristors. Nano Research. 2017;**10**:1584-1594

[76] Tian H, Zhao L, Wang X, Yeh YW, Yao N, Rand BP, et al. Extremely low operating current resistive memory based on exfoliated 2D perovskite single crystals for neuromorphic computing. ACS Nano. 2017;**11**:12247-12256. DOI: 10.1021/acsnano.7b05726

[77] Kang K, Ahn H, Song Y, Lee W, Kim J, Kim Y, et al. High-performance solution-processed organo-metal halide perovskite unipolar resistive memory devices in a cross-bar array structure. Advanced Materials. 2019;**31**:e1804841. DOI: 10.1002/adma.201804841

[78] Cheng X-F, Hou X, Zhou J, Gao B-J, He J-H, Li H, et al. Pseudohalide-induced 2D (CH$_3$NH$_3$)$_2$PbI$_2$(SCN)$_2$ perovskite for ternary resistive memory with high performance. Small. 2018;**14**:1703667. DOI: 10.1002/smll.201703667

[79] Kumar M, Kim H-S, Park DY, Jeong MS, Kim J. Compliance-free multileveled resistive switching in a transparent 2D perovskite for neuromorphic computing. ACS Applied Materials & Interfaces. 2018;**10**:12768-12772. DOI: 10.1021/acsami.7b19406

[80] Hu Y, Zhang S, Miao X, Su L, Bai F, Qiu T, et al. Ultrathin Cs3Bi2I9 nanosheets as an electronic memory material for flexible memristors. Advanced Materials Interfaces. 2017;**4**:2-9. DOI: 10.1002/admi.201700131

[81] Chen J-Y, Chiu Y-C, Li Y-T, Chueh C-C, Chen W-C. Nonvolatile perovskite-based photomemory with a multilevel memory behavior. Advanced Materials. 2017;**29**:1702217. DOI: 10.1002/adma.201702217

[82] Wang Y, Lv Z, Liao Q, Shan H, Chen J, Zhou Y, et al. Synergies of electrochemical metallization and valance change in all-inorganic perovskite quantum dots for resistive switching. Advanced Materials. 2018;**30**:e1800327. DOI: 10.1002/adma.201800327

[83] Tian H, Wang X, Wu F, Yang Y, Ren T-L. High performance 2D perovskite/graphene optical synapses as artificial eyes. In: 2018 IEEE Int. Electron Devices Meeting; IEEE. 2018. pp. 38.6.1-38.6.4

[84] Qian L, Sun Y, Wu M, Li C, Xie D, Ding L, et al. A lead-free two-dimensional perovskite for a high-performance flexible photoconductor and a light-stimulated synaptic device. Nanoscale. 2018;**10**:6837-6843. DOI: 10.1039/c8nr00914g